Materials Transactions, Vol. 43, No. 4 (2002) pp. 641 to 645
Special Issue on Radiation-Induced Effects by High Energy Particle/Solid Interaction

A Numerical Study on Composition Pattern Formation in Immiscible Alloys under Irradiation Condition

Yoshihisa Enomoto and Masataka Sawa *

Department of Environmental Technology, Nagoya Institute of Technology, Nagoya 466-8555, Japan

The kinetics of spontaneous composition pattern formation in a quenched alloys under irradiation is numerically studied by means of phenomenological Enrique-Bellon equation for the local concentration field. In the present model the irradiation effect is modeled as a ballistic mixing with an average distance of atomic relocation R and its frequency Γ. Several two-dimensional computer simulations show that the competitive mechanism between phase separation and irradiation-induced mixing might provide a novel way to stabilize and tune the steady-state nanostructures of phase separating materials in some region on (R, Γ) space.

(Received October 15, 2001; Accepted December 10, 2001)

Keywords: *irradiation, ballistic mixing, phase separation, spontaneous surface pattern formation, Enrique-Bellon model, nanostructures*

1. Introduction

The kinetics of phase transformations in materials driven far from thermodynamically equilibrium by an external driving force has recently attracted considerable attention. The term "driven systems" has been introduced to refer to these systems.[1)] A typical example of an evolving non-equilibrium system is given by materials under irradiation. Irradiation can create a variety of different phenomena, such as collision cascades, cascade damage, and radiation-enhanced diffusion, depending sensitively on the actual experimental condition.[2)] For metals and miscible alloy systems, experimental and theoretical study on irradiation effects have been done extensively.[1)] For instance, spontaneous formation of metallic nanostructures under irradiation have been recently observed in Au/SiO_2 and Pt/SiO_2.[3)] On the other hand, immiscible alloys under irradiation have, however, been less studied, since more complicated situations can be encountered through the interplay between irradiation and the internal kinetics in these systems.[2)]

In particular, an important but less studied case is ion-beam mixing of immiscible quenched alloys, where irradiation-induced ballistic mixing acts in opposition to thermodynamically driven kinetics like a spinodal decomposition. Each time an external particle collides with the solid, a local atomic rearrangement is produced. This rearrangement has a ballistic component that mixes the atoms regardless of their chemical identity, leading to bring the system to a random solid solution. During this ballistic mixing, a number of exchanges of atomic positions occur with an average relocation distance R and the frequency of these forced exchanges Γ, whose typical values are $R\sim10$ nm and $\Gamma\sim10^4\ s^{-1}$.[2)] To explore such competitive effects, the Cahn-Hilliard type dynamical equation for the local concentration field[4)] is known to provide a powerful tool, which has proposed by Enrique and Bellon.[5)] As far, their continuum model has been used only to discuss the linear stability analysis for the limiting case of spinodal decomposition from the unstable state under ballistic mixing.

In this work, we report on two-dimensional computer simulation results of Enrique-Bellon model, focusing on the long time behavior of compositional pattern formation. Especially, we will study the following effects on the morphology; (1) the average exchange range R, (2) the exchange frequency Γ, and (3) the initial homogeneous concentration S_i of the alloy. Despite the importance of controlling the compositional structures, these have been less studied previously, except for the mean field treatment and kinetic Monte Carlo simulation only for $S_i=0$.[6)] Numerical calculation of the continuum Enrique-Bellon model is computationally advantageous to study the large-scale and long-time properties of the system, compared with the kinetic Monte Carlo method. It is because the continuum model is based on the mesoscopic picture using the coarse-grained free energy, while the Monte Carlo simulation model is based on the microscopic picture.

2. The Model

We studied the spontaneous formation of compositional patterns in a quenched binary alloy with a positive heat of ballistic mixing under irradiation. The equation governing the time evolution of the system was given by Enrique and Bellon[5)]

$$\frac{\partial}{\partial t}S(\boldsymbol{r},\,t) = M\nabla^2[-2AS(\boldsymbol{r},\,t) + 4BS(\boldsymbol{r},\,t)^3 - 2C\nabla^2 S(\boldsymbol{r},\,t)] - \Gamma[S(\boldsymbol{r},\,t) - \langle S\rangle_R(\boldsymbol{r},\,t)] \tag{1}$$

where $S(\boldsymbol{r},\,t)$ is a local composition difference of the two constituents of the alloy at time t and position $\boldsymbol{r}$. Here, we have chosen the system free energy density as $-AS^2+BS^4+C(\nabla S)^2$ with positive coefficients A, B, and C, which are assumed to be constant as well as a mobility M in eq. (1). Estimation of these parameters would be required for the microscopic information about a specific system. The first term in the above equation represents the usual phase separation dynamics given by Cahn and Hilliard,[4)] and the second terms describes the forced mixing term due to irradiation with the frequency of atomic relocation Γ. In the second term, $\langle S\rangle_R$ represents a finite average of the concentration profile around

*Graduate Student, Nagoya Institute of Technology.

$\boldsymbol{r}$, given by

$$\langle S\rangle_R(\boldsymbol{r},\, t) \equiv \int S(\boldsymbol{r}',\, t) w_R(\boldsymbol{r}'-\boldsymbol{r}) d\boldsymbol{r}' \Big/ \int w_R(\boldsymbol{r}'-\boldsymbol{r}) d\boldsymbol{r}' \tag{2}$$

where the weight function $w_R(\boldsymbol{x}) \equiv \exp(-|\boldsymbol{x}|^2/(2R^2))$ denotes the distribution of atomic relocation distance with the average exchange distance R. In the model, for the sake of simplicity, the concentration of irradiation-induced point defects was assumed to have reached a steady value, and also the contribution of interstitials as well as defect sinks and clusters[7] was neglected. Moreover, non-ballistic mixing effects, any coupling between the degree of order and the concentration field[8] are not considered. Due to these assumptions, the above model excludes phenomena related to the order-disorder transition and macroscopic solute migration such as irradiation-induced heterogeneous precipitation. We focus on two-dimensional compositional patterning on the irradiated materials, neglecting the bulk diffusion and irradiation-induced phenomena occurring in the interior of the sample. These situations can be easily realized in thin film experiments with not too energetic cascades and some temperature region depending on the irradiated material properties[2] (*e.g.*, 1 MeV Kr ion irradiation in Ag–Cu thin films at temperature ranging from 80 to 473 K[9]). At least, the following two-dimensional simulation results might be applicable for the system with $D/\Gamma \ll R^2$ where D is the bulk diffusion constant, since the bulk diffusion-induced phenomena can be ignored in this case.

Now, it was discussed on the linear stability analysis of the initial homogeneous state. Similar analyses have been done for the case $S_i = 0$.[5] Linearizing eq. (1) about $S(\boldsymbol{r},\, t) = S_i$ in Fourier space, the equation for the fluctuations, $\tilde{S}(\boldsymbol{k},\, t) \equiv \int d\boldsymbol{r}[S(\boldsymbol{r},\, t) - S_i] \exp(-i\boldsymbol{k}\cdot\boldsymbol{r})$, has been obtained as

$$\frac{\partial}{\partial t}\tilde{S}(\boldsymbol{k},\, t) = [2M(A - 6S_i^2 B)k^2 - 2MCk^4 - \Gamma(1 - e^{-k^2R^2/6})]\tilde{S}(\boldsymbol{k},\, t) \tag{3}$$

with $k = |\boldsymbol{k}|$. The linear stability analyses of eq. (3) have shown that there are two characteristic values of Γ, denoted by Γ_1 and Γ_2, which depend on R and S_i. For $\Gamma > \Gamma_2$ the system is homogeneously mixed (solid solution), while for $\Gamma < \Gamma_1$ the homogeneous state is linearly unstable to grow, leading to macroscopic phase separation. For $\Gamma_1 < \Gamma < \Gamma_2$, certain modes k with $k_-^2 < k^2 < k_+^2$ are linearly unstable, suggesting a wave length selection at long times[5] (*i.e.*, the steady-state patterning). Moreover, an interval of the exchange frequency window $[\Gamma_1,\, \Gamma_2]$ decreases with R, reaching a zero value at a critical value R_c, when $\Gamma_1 = \Gamma_2$. Thus, the steady-state patterning is not possible for ballistic mixing with exchange distance smaller than R_c. For $R \gg R_c \equiv \sqrt{C/(A - 6S_i^2 B)}$, we obtain $\Gamma_1 = 2R^{-3}M\sqrt{(A - 6S_i^2 B)C}$, $\Gamma_2 = M(A - 6S_i^2 B + CR^{-2})^2/(2C)$, $k_- = 1/(2R)$, and $k_+ = \sqrt{0.5R_c^{-2} - 0.5R^{-2}}$. These analytic predictions have been partially confirmed by the kinetic Monte Carlo simulations only for the case $S_i = 0$.[6] The question is whether the similar results are obtained for the present continuum approach including the non-zero S_i case as well.

3. Simulation Results

Two-dimensional computer simulations of the phase separation dynamics under irradiation was carried out by changing values of S_i, Γ, and R. The system considered here is a two-dimensional plane, which corresponds to irradiated material surface. In the following simulations, we used the dimensionless variables such as $r_e \equiv R/L_0$ and $g \equiv t_0\Gamma$, by using the units of length $L_0 = \sqrt{C/A}$, time $t_0 = C/(2MA^2)$, and concentration field $S_0 = \sqrt{A/(2B)}$. The resulting dimensionless eq. (1) is solved numerically on a 256×256 square lattice with periodic boundary conditions, using a standard finite-difference scheme with mesh size being 0.5 and time step 0.01 Similar numerical procedure has been used in our previous work with different model.[10] The initial state of the system consists of a Gaussian random distribution of the concentration with the mean value S_i/S_0 and standard deviation 0.1.

First of all, the composition patterns, $S(x,\, y,\, t)/S_0$, with their amplitude along the x-axis, $S(x,\, y/L_0 = 64,\, t)/S_0$, are shown in Figs. 1–5 for the case $r_e = 8$ at $t/t_0 = 50$, 500, and 1000. The pattern evolution of $S(x,\, y/L_0 = 64,\, t)/S_0$ was also shown. In these figures, lattice points with $S(x,\, y,\, t)/S_0 < 0$ are plotted by dots. Note that for $r_e = 8$, we obtain $g_1 \equiv t_0\Gamma_1 = 0.0019$ and $g_2 \equiv t_0\Gamma_2 = 0.258$ for $S_i/S_0 = 0$, and $g_1 = 0.0016$ and $g_2 = 0.139$ for $S_i/S_0 = 0.3$, respectively. For $g = 0.0005$ ($< g_1$), usual macroscopic phase separation processes can be seen in Fig. 1 (spinodal decomposition with interconnected patterns at $S_i/S_0 = 0$) and in Fig. 4 (Ostwald ripening with droplet patterns at $S_i/S_0 = 0.3$). On

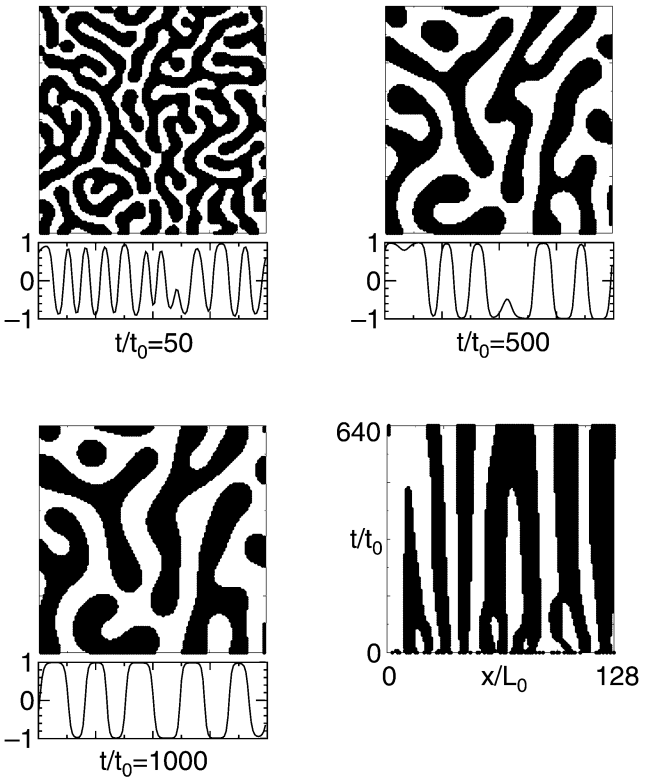

Fig. 1 Compositional patterns $S(x,\, y,\, t)/S_0$ with its amplitude, $S(x,\, y/L_0 = 64,\, t)/S_0$, for $r_e = 8$, $S_i = 0$, and $g = 0.0005$ at $t/t_0 = 50$, 500, and 1000. Dots are plotted at lattice points with $S(x,\, y,\, t)/S_0 < 0$. Time evolution of $S(x,\, y/L_0 = 64,\, t)/S_0$ is also shown.

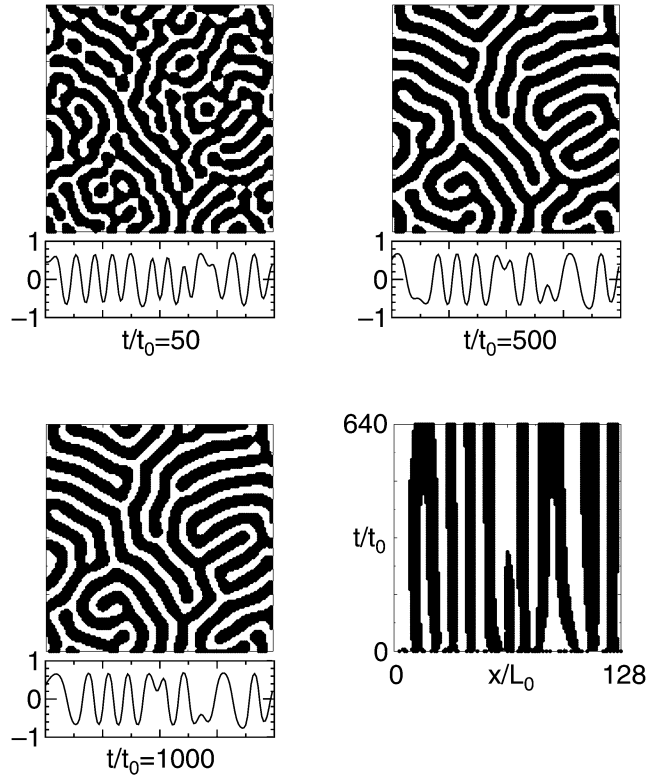

Fig. 2 Compositional patterns $S(x, y, t)/S_0$ with its amplitude, $S(x, y/L_0 = 64, t)/S_0$, for $r_e = 8$, $S_i/S_0 = 0$, and $g = 0.05$ at $t/t_0 = 50$, 500, and 1000. Dots are plotted at lattice points with $S(x, y, t)/S_0 < 0$. Time evolution of $S(x, y/L_0 = 64, t)/S_0$ is also shown.

Fig. 4 Compositional patterns $S(x, y, t)/S_0$ with its amplitude, $S(x, y = 64/L_0, t)/S_0$, for $r_e = 8$, $S_i/S_0 = 0.3$, and $g = 0.0005$ at $t/t_0 = 50$, 500, and 1000. Dots are plotted at lattice points with $S(x, y, t)/S_0 < 0$. Time evolution of $S(x, y/L_0 = 64, t)/S_0$ is also shown.

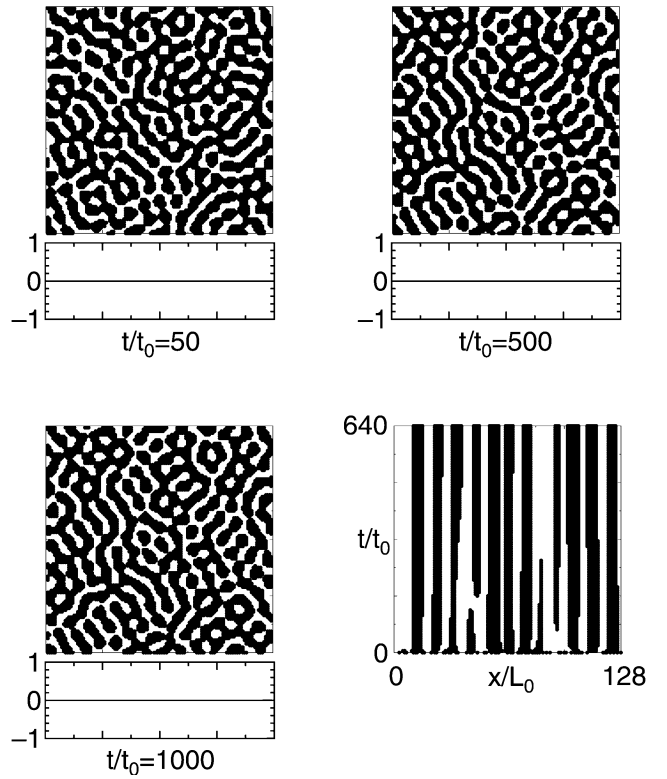

Fig. 3 Compositional patterns $S(x, y, t)/S_0$ with its amplitude, $S(x, y/L_0 = 64, t)/S_0$, for $r_e = 8$, $S_i/S_0 = 0$, and $g = 0.5$ at $t/t_0 = 50$, 500, and 1000. Dots are plotted at lattice points with $S(x, y, t)/S_0 < 0$. Time evolution of $S(x, y/L_0 = 64, t)/S_0$ is also shown.

Fig. 5 Compositional patterns $S(x, y, t)/S_0$ with its amplitude, $S(x, y/L_0 = 64, t)/S_0$, for $r_e = 8$, $S_i/S_0 = 0.3$, and $g = 0.05$ at $t/t_0 = 50$, 500, and 1000. Dots are plotted at lattice points with $S(x, y, t)/S_0 < 0$. Time evolution of $S(x, y/L_0 = 64, t)/S_0$ is also shown.

the other hand, a solid solution where $S(\boldsymbol{r}, t) \simeq S_i = 0$ even at long times, is observed in Fig. 3 for $g = 0.5$ ($>g_2$). The same behavior has been obtained for $S_i/S_0 = 0.3$ and $g = 0.5$, but this result is not shown here. For intermediate value of g at long times (here, $g = 0.05$ and $t \geq 500$), we can see the steady-state labyrinthine pattern at $S_i/S_0 = 0$ in Fig. 2 and the steady-state droplet patterns at $S_i/S_0 = 0.3$ in Fig. 5. These results are in agreement with theoretical analyses mentioned in the preceding section.

To analyze both the time evolution and long-time behavior of compositional patterns, we examine the structure factor of the system, $I(\boldsymbol{k}, t) \equiv \langle|\tilde{S}(\boldsymbol{k}, t)|^2\rangle$, where $\langle\cdots\rangle$ denotes the average over ten independent simulation runs. In the following discussion, we use the spherically averaged structure factor $I(k, t)$ and its characteristic wave number $\langle k\rangle$, which are defined by $I(k, t) = \int I(\boldsymbol{k}, t)d\Omega$ with $k = |\boldsymbol{k}|$ and solid angle Ω in $\boldsymbol{k}$-space, and $\langle k\rangle = \int kI(k, t)dk/\int I(k, t)dk$, respectively. Figures 6(a) and (b) show the averaged structure factor $I(k, t)$ at long time $t/t_0 = 500$, and the time evolution of the characteristic wave number $\langle k\rangle$, respectively, at $r_e = 8$ and $S_i/S_0 = 0$ for $g = 0.0005$, 0.05, and 0.5. The result at $g = 0.5$ is not shown in Fig. 6(b), since $\langle k\rangle L_0 \ll 1$ in this case. From Fig. 6 and other simulations with different parameter values, asymptotic behavior of structure factors is classified into three regimes corresponding to respective pattern morphology: (1) for phase separation regime, $I(k, t)$ has a single peak at a time-decreasing peak position, and the characteristic wave number decreases with time as $\langle k\rangle \sim t^{-1/3}$ (the well-known 1/3 growth law exponent); (2) for steady-state regime, $I(k, t)$ has a single peak, and the peak position and $\langle k\rangle$ gradually become constant, which correspond to the characteristic length of steady-state patterns; (3) for solid solution regime, $I(k, t) \simeq 0$, which corresponds to a homogeneous state. For the steady-state regime, $\langle k\rangle$ is found to be an increasing function of g as is shown in Fig. 7(a). From Fig. 7(b) with further simulations, we also find a scaling relation between $\langle k\rangle$ and r_e for $r_e \geq 8$ as $r_e\langle k\rangle L_0 = F(gr_e^3)$ with a scaling function $F(x)$. Such scaling behavior has been predicted theoretically for large r_e,[5] but this is the first evident confirmation. Finally, we note that the similar results have been obtained for the non-zero S_i case as well.

Since we have obtained $\langle k\rangle L_0 \sim 0.6$ in the present simulation at $g = 0.005$, $r_e = 8$ and $S_i = 0$, and also $R_c \sim 0.1$ nm in most experiments,[2] the characteristic wave length of the steady-state pattern in this case is estimated as $2\pi/\langle k\rangle \sim 1$ nm. Thus, the irradiation might be used as a processing tool

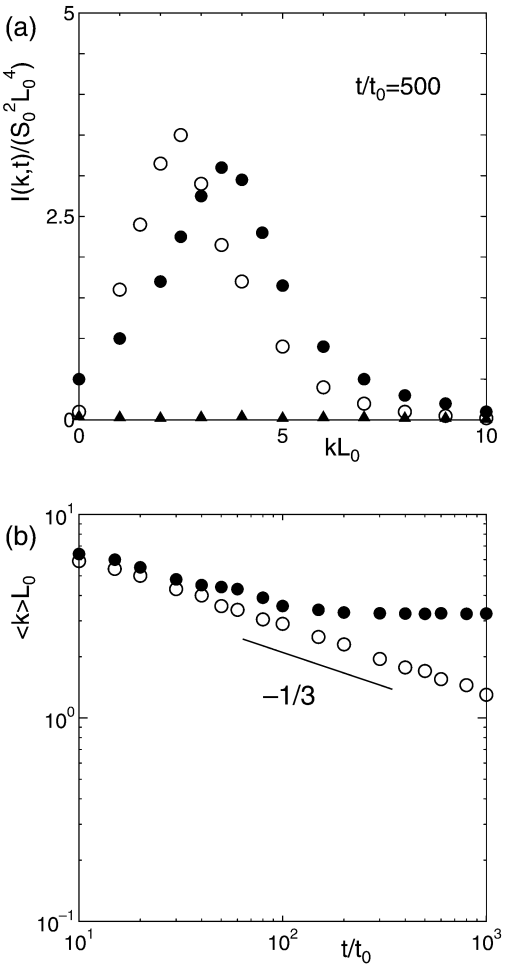

Fig. 6 (a) Spherically averaged structure factor $I(k, t/t_0 = 500)/(S_0^2L_0^4)$ at $S_i/S_0 = 0$ and $r_e = 8$ for $g = 0.0005$ (◯), 0.05 (●), and 0.5 (▲). (b) Time evolution of the characteristic wave number $\langle k\rangle L_0$ at $S_i/S_0 = 0$ and $r_e = 8$ for $g = 0.0005$ (◯), and 0.05 (●). The slope of a line indicates the value of temporal power law exponent of $\langle k\rangle$.

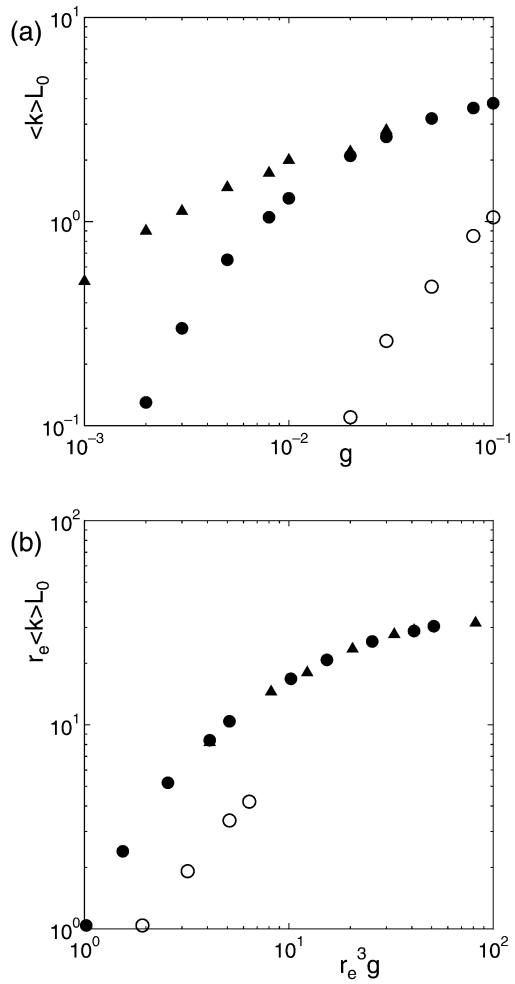

Fig. 7 (a) Characteristic wave number $\langle k\rangle L_0$ for the steady-state patterns at $S_i/S_0 = 0$ as a function of g for $r_e = 4$ (◯), 8 (●), and 16 (▲). (b) Scaling relation between $\langle k\rangle L_0$ and g for the steady-state patterns at $S_i/S_0 = 0$ for $r_e = 4$ (◯), 8 (●), and 16 (▲).

to synthesize nanostructures in a self-organized manner. The present simulation is restricted to the two-dimensional case. However, as is similar to the case of the simple phase separation dynamics,[11] the qualitative properties of the system such as the existence of scaling behavior and occurrence of the steady-state regime are expected to be appropriate even for the three-dimensional case. On the other hand, the detailed features such as the explicit form of scaling function and onset time of the steady-state regime might depend on the dimensionality.

4. Conclusion

In summary, we have numerically studied the two-dimensional phase separation dynamics of quenched alloys driven by irradiation, where the phase separation dynamics competes with the irradiation-induced ballistic mixing. This is the first simulation study of the continuum Enrique-Bellon model. From several simulation results it has been found that the irradiation-induced ballistic mixing can affect the dynamical process of phase separation in various manners, and it might provide a novel way to control the steady-state compositional morphology of phase separating materials under some irradiation conditions. Thus, the present model has been shown to be useful and potentially rich to examine appropriate experimental conditions to create a favorable steady-state nanoscale pattern morphology, at least in a phenomenological level.

In the present work we have concentrated on rather simplified situation. In order to compare simulation results with real experimental data, both of further simulation study including other important factors neglected here (as was mentioned in Sec. 2) and further theoretical analysis of numerical results are needed, as well as estimations of phenomenological parameters in the model. These are left for future study.

REFERENCES

1) G. Martin and P. Bellon: Solid State Phys. **50** (1997) 189–273.
2) K. C. Rusell: Prog. Mater. Sci. **28** (1984) 229–271.
3) X. Hu, D. G. Cahill and R. S. Averback: Appl. Phys. Lett. **76** (2000) 3215–3217.
4) J. W. Cahn and J. E. Hilliard: J. Chem. Phys. **28** (1958) 258–267.
5) R. A. Enrique and P. Bellon: Phys. Rev. Lett. **84** (2000) 2885–2888.
6) R. A. Enrique and P. Bellon: Phys. Rev. B **63** (2001) 134111.
7) S. L. Dudarev: Phys. Rev. B **62** (2000) 9325–9337.
8) G. Schmitz, J. C. Ewert, F. Harbsmeier, M. Uhrmacher and F. Haider: Phys. Rev. B **63** (2001) 224113.
9) L. C. Wei and R. S. Averback: J. Appl. Phys. **81** (1997) 613–623.
10) Y. Enomoto: Thin Solid Films **369** (2000) 21–24.
11) A. J. Bray: Adv. Phys. **43** (1994) 357–459.